Article

Steady-State Risk Prediction Analysis of Power System Based on Power Digital Twinning

Qiang Li [1],*, Feng Zhao [1], Li Zhuang [2], Qiulin Wang [2],* and Chenzhou Wu [2]

1   State Grid Information & Telecommunication Group Co., Ltd., Beijing 102211, China
2   Fujian Yirong Information Technology Co., Ltd., Fuzhou 350001, China
*   Correspondence: qiang-li@sgitg.sgcc.com.cn (Q.L.); wqllwq@126.com (Q.W.)

Abstract: In essence, electric digital twinning uses artificial intelligence technology to model complex electric power systems, and is the development and supplement of electric power modeling technology. This paper intends to predict and analyze the steady-state risks of complex power systems based on the power digital twin. Firstly, power flow calculation and optimization are carried out for complex large power grid systems. Based on sparse matrix storage and node coding optimization, the power flow calculation speed is improved and the memory usage is reduced. The accuracy and timeliness of the continuous power flow calculation when obtaining the node power and voltage are improved by using the unit processing tangent prediction vector and the internal machine of the prediction vector to determine the prediction direction. Secondly, according to the optimization results of the power flow calculation, the multi-objective optimization problem of power system simulation is solved by using the advantages of neural network modeling, such as self-learning, self-adaptation, fault tolerance, and parallelism. Finally, the power flow calculation optimization and neural network analysis are applied to the integrated stability program of the United States Western Combined Power Grid (WSCC) power system's nine-node model; this is in order to simulate the regional power grid for simulation analysis. Different risks in the power system under steady–state conditions are predicted and analyzed, the voltage drop in the transient voltage is reduced under multiple working conditions, and the relative power angle is improved, improving the overall stability of the power system.

Keywords: power flow optimization; steady-state risk; digital twinning; neural networks; stability

1. Introduction

The fundamental and long-term value of digital twinning, in terms of modeling and simulation technology, goes far beyond its technical domain in the use of artificial intelligence technology to model complex power systems; this is a development and complement to power modeling technology [1–4]. The current situation of high cost and low efficiency cannot meet the demand of electric digital twin research, and an efficient and low-cost modeling method is the main way to solve this problem.

Whether at home or abroad, the application of digital twin technology in the power system and energy industry is mostly in the stage of exploration and verification. In terms of the concept and framework design of power system digital twinning, the literature [5–9] combines the definition of digital twinning with the characteristics of an Energy Internet, proposes the concept of Energy Internet digital twinning, proposes the construction methods and possible application scenarios of Energy Internet digital twinning, and details the key problems solved by digital twinning technology, taking Energy Internet planning as an example. The literature [10–13] proposes the concept of electric digital twinning and designs a data-driven electric digital twinning framework that combines traditional model-driven and expert systems. The literature [8] defines the overall framework and technical route of an Energy Internet digital twin system. The literature [14–16] describes the basic connotation, technical characteristics, and challenges of digital twinning in integrated energy systems. The literature [17–20] proposes a safety analysis framework based

on the digital twin system, which provides real-time data visualization and realizes the operation status monitoring and evaluation of each energy generation system in the power system. The literature [21–23] discusses the application status and the prospect of digital twin technology from the aspects of power grid operation and power equipment.

In terms of actual modeling, the literature [24] establishes a multi-node power system model and proposes the influence principle of a power system based on digital twinning. In the literature [25], digital twinning and the multi-agent control architecture of microgrids are proposed to intellectualize the power grid. The paper [26] constructs the digital twin system of the active power prediction system to predict the power of short-term power systems. In the literature [27], the digital twin model is adopted to estimate the operating characteristics of the system under a steady state in real-time, and fault estimation is carried out based on it. In the literature [28], the digital twin model is applied to energy system detection. The literature [29] uses the digital twin model to estimate the state of the electric power system. To sum up, the application of digital twinning technology in power systems is still in the stage of theoretical exploration, and there are few practical systems designed to solve the practical production problems of the complex large power grid. With the increasing complexity of power systems, the regulation and control of large power grids is becoming increasingly complex, and more refined and intelligent scheduling and decision-making tools are urgently needed. Therefore, the mirroring feature of the digital twin to the physical system applies to the field of real-time control of the power grid, which is helpful in order to improve the accuracy and real-time nature of the dispatching operation decision of the power grid. [30–34] Digital twins require real-time and two-way communication between the digital model and the physical system. In the actual application of this article, the NETCONF protocol will be used, and the RPC-based mechanism will provide a set of network device configurations between the client and the server; this system, has settings that can be added, modified, and deleted, a framework mechanism for querying the configuration, status, and statistics, and can be used as a network administrator or network configuration application with network devices and logical connections between them. NETCONF can transmit two types of information: configuration data and state data.

- This paper innovatively proposes a power flow calculation optimization method for a complex large power grid system, including improving the speed of power flow calculation and reducing the use of memory; this is based on sparse matrix storage and node coding optimization, uses the unit processing tangent prediction vector, and determines the prediction direction by the machine in the prediction vector in order to improve the accuracy and timeliness of continuous power flow calculation when obtaining node power and voltage.
- In addition, the optimization results of power flow calculation are innovatively introduced into the multi-objective optimization of neural network analysis, and the risk prediction analysis of the steady-state power system is carried out.
- To verify the rationality of the proposed power flow optimization method and the multi-objective neural network algorithm in the complex power system, the proposed algorithm is innovatively introduced into the WSCC nine-node model in the integrated stability program of the power system; this is performed in order to simulate the regional power grid, the accuracy of the proposed power flow optimization method, and to verify the multi-objective neural network risk prediction. The risk of a complex power system is reduced based on the power digital twin.

2. Study on Optimization and Improvement of Power Flow Calculation

The improvement and optimization of power grid real-time computing modeling technology for simulating power flow is researched to form a reliable convergence for different systems and different operating conditions; this includes a small memory consumption, a fast computing speed, and an ease of adjustment and modification. Power flow calculation is the most basic calculation in power system analysis [35–38]. It is also the basis of power system optimization, as well as operation, planning, safety and reliability analysis. The

power flow calculation model for the same power grid simulation system is also the basis and starting point of all other computational analyses; this is to ensure that the real-time power flow calculation is as fast as possible in order to achieve a realistic effect. This is the most effective way to solve the current complex power system simulation to further optimize the power flow calculation technology [38–40].

This section focuses on improving the accuracy and timeliness of continuous power flow calculation when obtaining Nodal power and voltage; this uses matrix sparse storage and node coding optimization methods to improve the speed of the power flow calculation, reducing the use of memory to treat the tangent prediction vector in the unit, and determining the prediction direction via the machine in the prediction vector.

As the power flow calculation is iterative, the coefficient matrix is directly related to the number of nodes in the calculation speed. In order to accurately predict the nodal power and the voltage for the power flow solution that is close to the critical point, the change in the state quantity (V, θ) of each power flow calculation is increased; this results in the error of parameter transfer and a larger modulus value for the tangent prediction vector. If the modulus of the tangent prediction vector exceeds a certain range, the prediction algorithm will no longer satisfy the principle of approximation, resulting in the non-convergence of the correction operation and a failure in the power flow calculation. This section mainly realizes power flow calculation optimization from three directions: the sparse matrix, node coding optimization, and the processing of the tangent prediction vector unit. Figure 1 shows the technical route of accelerated optimization of power flow calculation.3. Results.
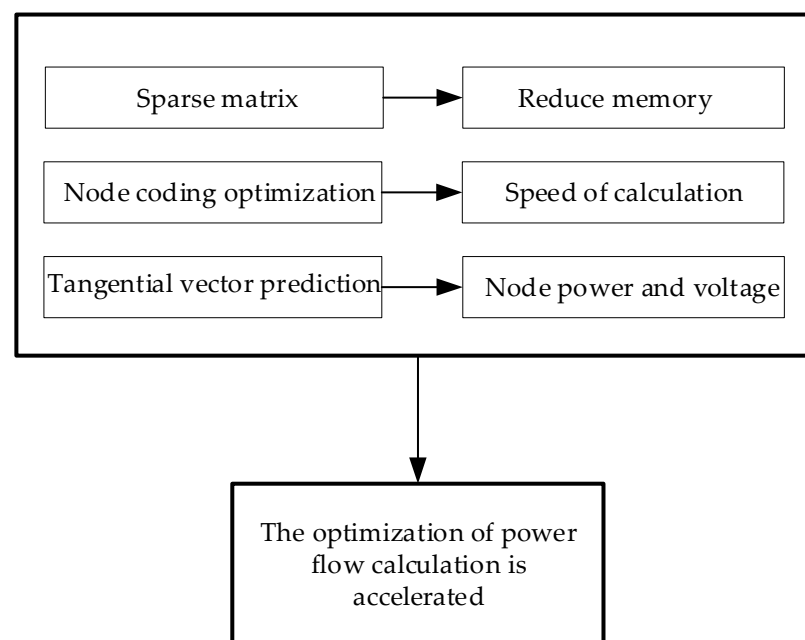

Figure 1. Technical route of accelerated optimization for the power flow calculation.

2.1. Sparse Storage Analysis

According to the characteristics of the matrix, namely high symmetry and sparsity, the more nodes, the higher the sparsity. Therefore, we can use the sparse technique to store and calculate only non-zero elements to save time and memory. Storage admittance matrix each row of non-zero elements (triplet notation) for the whole array storage, has greatly reduced the amount of storage. Its advantage is that the calculation speed is fast [41–43], and the approximate calculation process is as follows:

(1) The corresponding triples in the a.ATA are found for transposition, according to the row order of the B matrix.

(2) Quick transpose: the triples are transposed in the order of the a.data, and the transposed triples are placed in the appropriate position of the b.data.

(3) Calculation of the appropriate position: Firstly, the number of non-zero elements in each column of the M matrix (that is, each row of T) is calculated, and then the position of the first non-zero element in each column of the M matrix in the b.data is calculated.

The basic algorithm steps can be summarized as follows:

Two vectors are set: num[col], the number of non-zero elements in the col column, and cpot[col], the appropriate position of the first non-zero element in the col column in the b.data; This indicates the position of the next non-zero entry in the b.data for that column during the transposition.

A simple B matrix is set, as shown in formula (1):

$$\begin{bmatrix} B_{11} & B_{12} & 0 & B_{14} \\ B_{21} & B_{22} & B_{23} & 0 \\ 0 & B_{32} & B_{33} & 0 \\ B_{41} & 0 & 0 & B_{44} \end{bmatrix} \quad (1)$$

The diagonal elements are recorded with the one-dimensional array bdia, as shown in Figure 2 below.
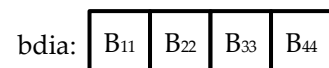
bdia: | B_{11} | B_{22} | B_{33} | B_{44} |

Figure 2. The one-dimensional array bdia records the diagonal elements.

A one-dimensional array is used to record the non-zero elements of the off-diagonal elements, as shown in Figure 3 below, and a one-dimensional array bdia records the off-diagonal elements.
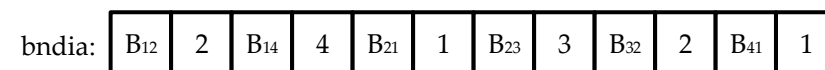
bndia: | B_{12} | 2 | B_{14} | 4 | B_{21} | 1 | B_{23} | 3 | B_{32} | 2 | B_{41} | 1 |

Figure 3. The application of the non-one-dimensional array bdia to record diagonal elements.

A one-dimensional array is used to record the non-zero elements of the non-diagonal elements. The bdia records the non-zero elements of the odd dimension and the even dimension of the second corner code of this element. Note that the storage of the non-zero elements of each row in the matrix must be adjacent to the storage. Then, a single-dimensional array is used to record each line of non-zero elements in the storage of the starting position and the end position. In Figure 4, the single-dimensional array Pnum is used to record the start and end positions of each row of non-zero elements stored in the store.

Pnum: | 0 | 4 | 8 | 10 | 12 |

Figure 4. The use of the one-dimensional array Pnum to record the starting and ending positions of each row of non-zero elements stored in the store.

As can be seen from the above process, Pnum (i) +1 is the storage starting position of the non-zero elements in the ith row of matrix B in bdia, and Pnum (i+1) is the storage ending position. (Pnum (i+1) − Pnum (i)) /2 is the number of non-zero elements in row i. The Pnum array makes it easy to find a specific non-zero element.

2.2. Research on Node Coding Optimization

At present, node optimization numbering mainly includes static optimization methods, semi-dynamic optimization methods, and dynamic optimization methods. Compared with these three optimization methods, the static optimization method has a simple program,

but the optimization effect is not good. The dynamic optimization method has the best effect, but the optimization speed is slow and the optimization program is complex, while the semi-dynamic optimization method has the advantages of a good optimization effect, a simple optimization program, and a fast optimization speed. [44–48]

The computational efficiency of the sparse vector method can be improved based on the semi-dynamic optimization method. A special numbering method can be adopted to make the branches of the road tree on the final directed factor graph as short as possible. In this way, when sparse vector technology is used, the path of the fast previous generation and the back generation is shorter, which reduces the calculation amount of the previous generation and back generation.

With the node optimization number, the specific process is as follows: The adjacency matrix is formed according to the topology structure of the power grid, and the num array is used to record the number of branches connected by each node. The node number with the fewest connections is found and stored in the array line. When the number of connected nodes is the same, the number in the smaller sequence is taken and stored in line. The number of branches added or subtracted after node elimination is modified, and the value of the array number is updated. The corresponding node in the matrix of the row and column is eliminated. The second step is returned to, and the node is repeatedly eliminated. The position of the balance node in the line is adjusted, and the number of the balance node is placed in the last position of the line.

The specific optimization steps are as follows: the first step determines whether the sum of the degrees of the compared nodes is greater than 3. If yes, the one with the minimum degree is selected; otherwise, the second step is entered and the one with the minimum length is selected. In the third step, the one with the smallest increment to the total network length after elimination is chosen. In the first step, if the sum of the degrees of the two comparison nodes is less than or equal to 3, then the second step is turned to. This equates to the status of the nodes of degree 1 and degree 2. In the third step, the influence of node J on the total length of the network is eliminated.

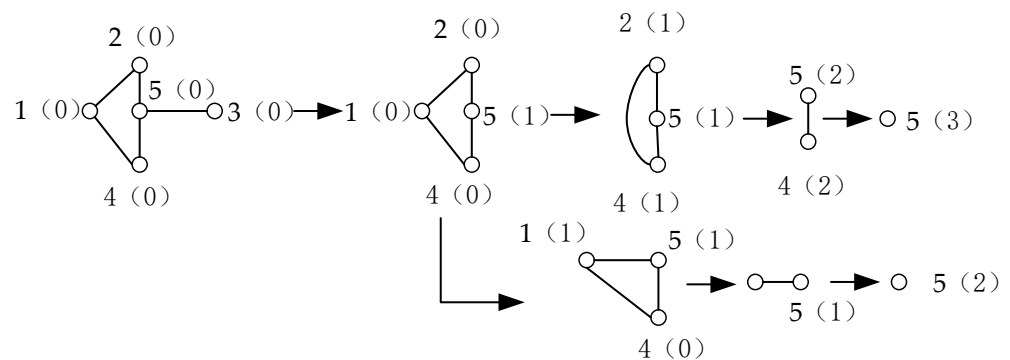Figure 5 shows the topology of a 5–node network.

Figure 5. The 5-node network topology.

First, the tree of node 2 is eliminated, as shown in Figure 6 below, that is, the tree of node 2 is eliminated.
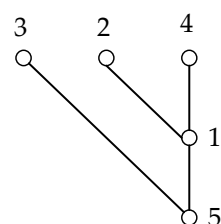

Figure 6. The elimination of the tree for node 2.

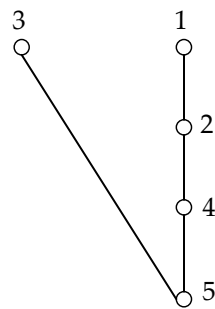Then, the tree of node 1 is deleted, as shown in Figure 7 below.

Figure 7. The elimination of the tree for node 1.

The solution of eliminating node 2 first is better because, when eliminating node 2, the length of node 1 is only increased by 1; meanwhile, when eliminating node 1 first, the length of node 2 and node 4 is increased. It can be seen that the elimination of nodes first increases the total length of the whole network, or makes the network "tree" develop deeper faster, which is unfavorable for the fast regeneration and back generation.

2.3. Research on the Unit Processing of Tangent Vector

The prediction algorithm should follow principles. The principle is the principle of approximation, that is, the predicted value should be close enough to the corresponding exact value in the prediction process. The predicted value at i+1 is more approximate than the predicted value at i. For the tangent prediction algorithm with local parameterization, the closer the power flow calculation is to the node power and voltage, and to the critical point of the line, the larger the modulus of the tangent prediction vector will be, resulting in a larger error caused by parameter transfer. If the modulus of the tangent prediction vector exceeds a certain range, the prediction algorithm will no longer satisfy the principle of approximation, resulting in the non-convergence of the correction operation and the failure of the power flow calculation.

To make the prediction algorithm meet the principle of approximation, the prediction vector can be unitized, that is, in the more curved part of the node power and voltage, the modulus value of the tangent prediction vector can be a unit quantity. Unit processing is conducive to ensuring the approximation of the prediction algorithm.

To meet the directionality requirements of the prediction algorithm, the inner product of the two adjacent tangent prediction vectors can be used to determine the direction of the continuous power flow solution; therefore, the positive direction of the inner product operation is the same as that of the previous step, and the negative direction of the inner product operation is the opposite direction of the previous step. When the inner product operation result of the two-step tangent prediction vector is greater than 0, the budget publicity is formula (2); if the result is less than 0, the budget publicity is formula (3).

$$\left(X^{i+1}, \lambda^{i+1} \right) = \left(X^i, \lambda^i \right) + \sigma \frac{\left(dX^i, d\lambda^i \right)}{\| \left(dX^i, d\lambda^i \right) \|} \tag{2}$$

$$\left(X^{i+1}, \lambda^{i+1} \right) = \left(X^i, \lambda^i \right) - \sigma \frac{\left(dX^i, d\lambda^i \right)}{\| \left(dX^i, d\lambda^i \right) \|} \tag{3}$$

3. Artificial Neural Network Analysis

3.1. Artificial Neural Network Method

Neural networks are composed of simple units that operate in parallel and are triggered by the biological nervous system. The function of the network is determined by the

interconnection between the units. We can train the neural network to adjust the connection strength (weight) between the units to fulfill the specified function. [49–52]

Usually, neural networks are trained and adjusted to make a specific input lead to a specific output. This can be illustrated by the figure below, [53–56] in which the network is trained by constantly comparing the output and the target value until the network output and the target value are the same. Usually, the network has many of these input–output pairs in this supervised training mode. Figure 8 below shows the learning process of the neural network.
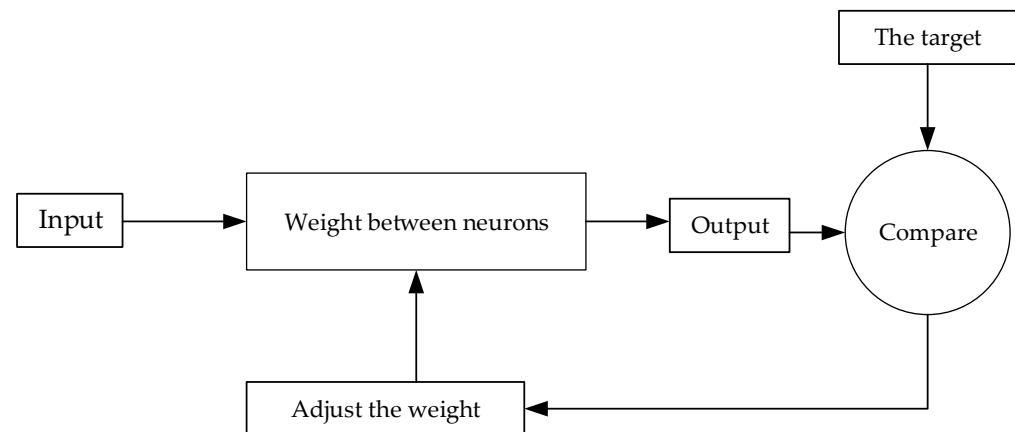
Figure 8. Learning process of neural network.

An artificial neural network is a nonlinear data-processing method, used to simulate human neurons, which is a transformation and abstraction of the natural biological nervous system. The neural network is mainly composed of neurons. As shown in Figure 9, there is a nonlinear correlation between the input and output of each neuron, and such an extensive connection among all the neurons eventually forms a complete complex nonlinear network. The method simulates the functions of signal transmission, processing, retrieval, and storage of the human nervous system, and realizes the nonlinear reflection of the body inch, from X dimension space to Y dimension space.
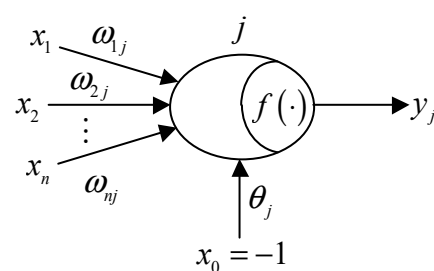

Figure 9. Artificial neuron structure model.

The artificial neural network method has the advantages of simple modeling, nonlinear implicit expression, high parallelism, and strong fault tolerance, so it is often used in the prediction of power loads. This method has a strong adaptive ability for some non-precise laws and non-structural data, and can learn independently, memorize information [57,58], optimize calculation and reason knowledge, etc.; these not possessed by other algorithms.

In actual life, the power load is mainly affected by the season, temperature, holidays, and other factors, and these factors are random with a large number of data without linear relationships. At the same time, it is necessary to construct nonlinear relations for some voltage and frequency disturbances with large spans. It is difficult to model these large, non-linear data with some obvious mathematical expression and explain how the data changes. The characteristics of the nonlinear implicit expression of an artificial neural network

can precisely solve this difficulty [59–62]. The neuron is like a black box, replacing the functional relationship between a large number of data information into a high-dimensional nonlinear mapping relation; the independent variable in the functional relation becomes the input quantity and the dependent variable becomes the output quantity, finally solving the problem of the nonlinear relationship between various influencing factors [63,64]. The artificial neural network method is not only suitable for short- and ultra-short-term load forecasting, but also helpful for medium- and long-term load forecasting.

At present, the artificial neural network can be divided into the following models through different interconnection modes: the forward network, the forward network with output feedback, the forward network with intra-layer interconnection, the fully interconnected network, and the locally interconnected network. The forward network topology with output feedback is used in this paper, and is shown in Figure 10 below:
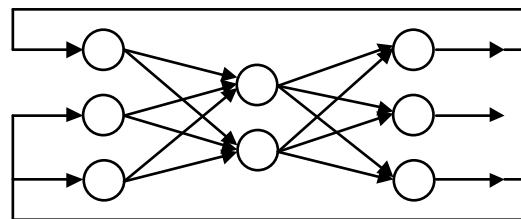

Figure 10. Forward network topology of output feedback.

Figure 10 shows the forward network topology of the output feedback in the interconnected artificial neural network. The data information of the output layer will be fed back to the input layer, which means that each node of the input layer not only needs to receive the external input information, but also may receive the feedback information output by the neurons of the output layer. This mode is more suitable for storing pattern sequences and neurocognitive machines.

In addition, the local interconnected network is also one of the interconnected artificial neural networks. Different from the fully interconnected network, the neurons in this type only have input and output relationships with the neurons in one or several layers around them, forming a local feedback network structure. The most commonly–used local interconnected network is the Elman network.

3.2. Process of Applying Artificial Neural Network Algorithm

The flow of the artificial neural network algorithm is as follows:

The objective function of this paper is to minimize the instantaneous increment of voltage and power. Both the active power loss and generator reactive power can be expressed as the function form of control variables. The objective function can be expressed in an incremental form, linearized as follows:

$$\min \Delta f(\Delta X_C) = \frac{\partial f}{\partial V_G} \cdot \Delta V_G + \frac{\partial f}{\partial T_K} \cdot \Delta T_K + \frac{\partial f}{\partial Q_C} \cdot \Delta Q_C \tag{4}$$

where ΔX_C represents the increment of the control variables,

$f(X_C)$ represents the partial derivative of the generator voltage, transformer ratio and reactive power compensation $\frac{\partial f}{\partial V_G}, \frac{\partial f}{\partial T_K}, \frac{\partial f}{\partial Q_C}$, and $\Delta V_G, \Delta T_K$ and ΔQ_C represent the increment of the generator terminal voltage, the increment of the transformer ratio and the increment of the reactive power compensation equipment, respectively.

(1) The population is initialized and $Q(t_0)$ randomly generates N-bits encoded by a neural network $q_j^{t_0}$. The artificial neural network algorithm is, firstly, needed to initialize the population $Q(t_0)$, and to initialize the bit codes of two neural networks $\left(\alpha_i^{t_0}, \beta_i^{t_0} \right)$ of n

neural networks in the population $\left(1/\sqrt{2}, 1/\sqrt{2}\right)$; this indicates that all possible states are equally probable, as is evident in the following:

$$\left| \Psi_{q_j}^{t_0} \right\rangle = \sum_{k=1}^{2^m} \frac{1}{\sqrt{2^m}} |S_k\rangle \tag{5}$$

(2) All the individuals included in the population are measured once to obtain a definitive set of solutions p(t), where $p(t) = \left\{ p_1^t, p_2^t, \ldots p_n^t \right\}$ represents solution number one in the population of generation t. The measurement result is $j(j = 1, 2, \cdots, n)$, which is the probability OR of randomly generating the interval number and comparing it with the neural network bit. If it is greater than OR, the measurement result is 1; otherwise, it is 0.

(3) Based on the established fitness function (objective function), the fitness evaluation is carried out for each determined solution, and the optimal individual and the corresponding fitness value are recorded.

(4) The rotation angle adjustment strategy of the neural network revolving door is used to calculate the rotation angle of the neural network and update the neural network revolving door. This article uses a general, problem-independent tuning strategy, where x_i and best$_i$ are the position of the current individual and the current optimal individual, respectively; $f(x)$ss the objective function; $\Delta\theta_i$ is the magnitude of the rotation angle; and $s(\alpha_i, \beta_i)$ is the direction of the rotation angle, namely, the symbol of θ_i. The adjustment strategy is used to compare the fitness value of the current individual with the fitness value of the current optimal individual in the population. The larger the objective function value is, the better the individual is, then $f(x) > f(best)$ and the corresponding bit of the neural network is adjusted to make the probability amplitude approximate to the direction of x. Otherwise, it is approaching in the direction of the best$_i$.

(5) Whether the calculation process can be terminated is determined. If the termination condition is met, the calculation ends. Otherwise, the number of iterations updates the population with the revolving door of the neural network, and the algorithm moves to step (2).

In this paper, the steady-state and transient characteristics of the regional power system are fully considered, and the evaluation index of the evaluation configuration strategy is established based on the voltage transient characteristics of different nodes after failure, which can more truly reflect the voltage dynamic characteristics of the regional power system. Moreover, the simulation software is used to continuously optimize the steady-state and transient operation mode, to obtain a real and rel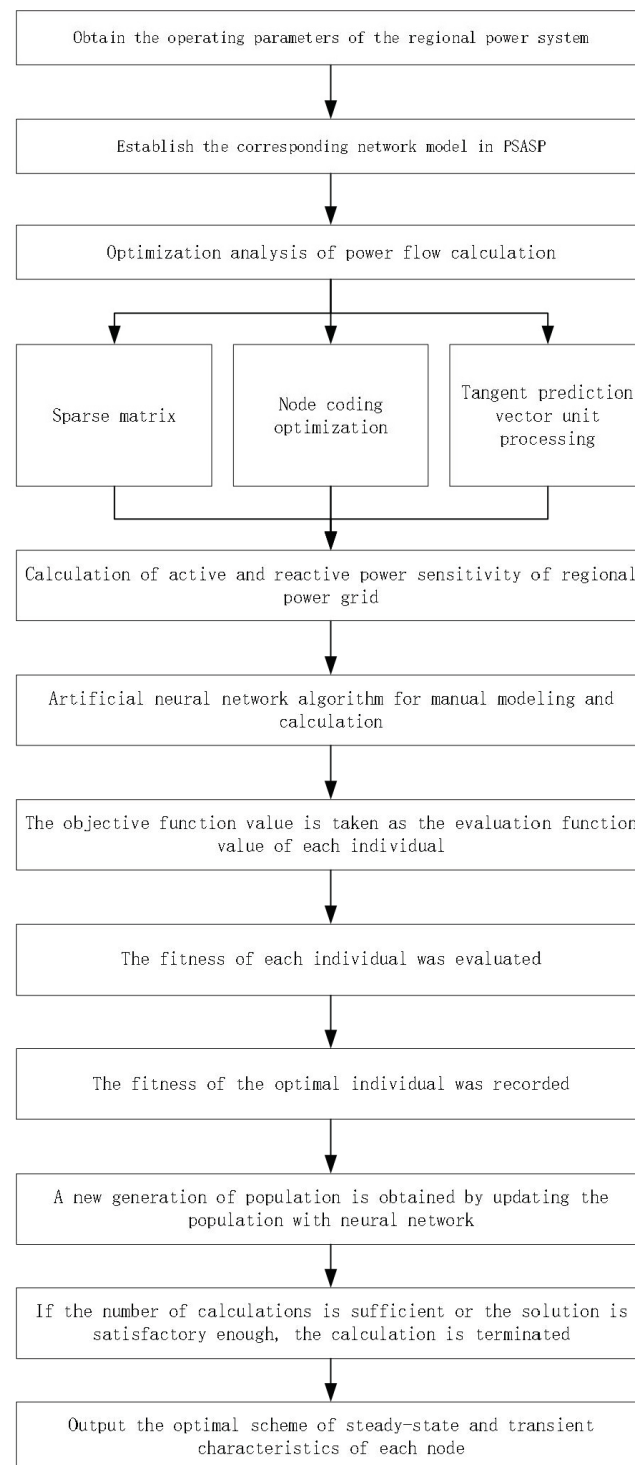iable optimal active and reactive power configuration strategy. Figure 11 shows the general flow chart of steady-state risk prediction analysis by digital twinning in the regional power network. The specific calculation steps are as follows:

(1) The operating parameters of the regional power system are obtained, and the corresponding network model is established in PSASP;

(2) The power flow calculation optimization analysis involves the sparse matrix, node coding optimization, and tangent prediction vector unit processing;

(3) The active power and reactive power sensitivity of the regional power grid are calculated;

(4) Artificial modeling and calculation, according to the artificial neural network algorithm, is conducted, the initial population and the calculation parameters of the neural network algorithm are determined, namely the initial defense strategy of each node, and this is revised in PSASP;

(5) The dynamic simulation of the calculation is carried out. In the actual calculation process, the steady-state index in the objective function is ignored, but only the transient index is retained; the objective function value is taken as the evaluation function value of each individual;

(6) The above calculation is made for each individual in the initial population;

(7) the fitness of each individual is evaluated;

(8) the fitness of the optimal individual is recorded;

(9) A new generation of the population is obtained by programming and updating the population with the revolving gate of the neural network;

(10) The new population is taken as the initial population, (4) is returned to, and the above calculation is repeated;

(11) If the termination condition is satisfied, that is, if the number of calculations is sufficient or the solution is satisfactory enough, the calculation is terminated (12). The optimal scheme of the transient characteristics of each node is output.

Figure 11. General flow chart of steady-state risk prediction analysis by digital twinning in the regional power network.

4. Simulation Verification Analysis Based on Multi-Node Network

4.1. Nine-node Power Network with a WSCC-Integrated Stability Program Introduction

Figure 12 shows the power flow calculation and analysis of a nine-node power network with a WSCC-integrated stability program under a steady state. It can be seen that the power flow distribution of each unit and network is uniform, and that the system runs stably.
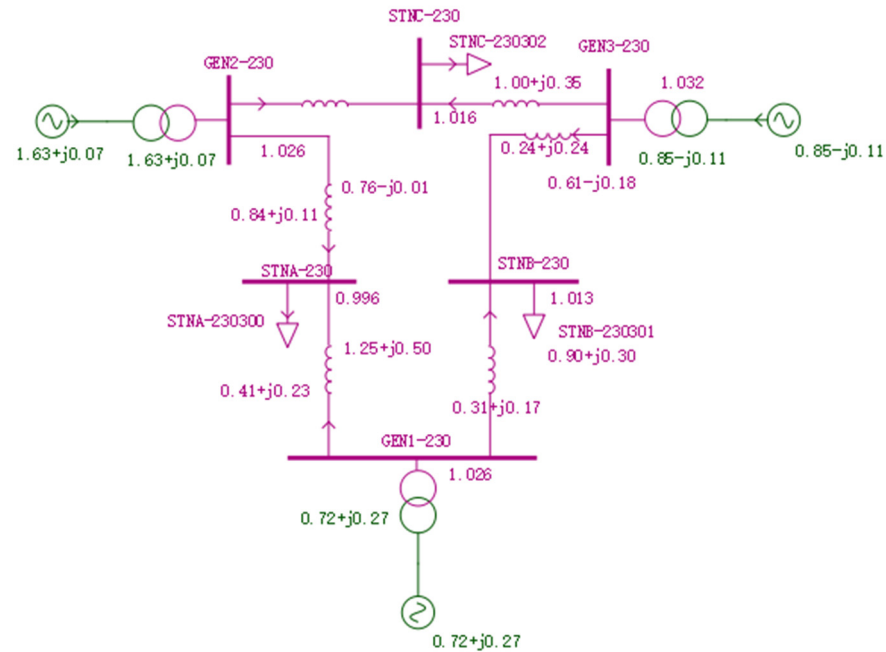
Figure 12. Power flow calculation and analysis of a nine-node power network with integrated stability program WSCC under a steady state.

The three-machine, nine-bus system of the Western Power System (WSCC) in the United States is a classic example of power system research. Table 1 below shows the bus data of the nine-node WSCC power network-integrated stability program under a steady state. The following Table 2 shows the AC line data of the nine-node WSCC power network-integrated stability program under steady-state conditions.

Table 1. Bus data.

BUS_NAME	PHYPOS	Plant/Station	BASE_KV	VMAX_KV	VMIN_KV
GEN1	0	Gen1	16.5	18.15	14.85
GEN2	0	Gen2	18	19.8	16.2
GEN3	0	Gen3	13.8	15.18	12.42
GEN1–230	0	Gen1	230	0	0
GEN2–230	0	Gen2	230	0	0
GEN3–230	0	Gen3	230	0	0
STNA–230	0	STNA	230	0	0
STNB–230	0	STNB	230	0	0
STNC–230	0	STNC	230	0	0

Table 2. AC line data.

NAME	I_NAME	J_NAME	R1	X1	B/2	R0	X0
AC_1	GEN1–230	STNA–230	0.01	0.085	0.088	0	0.255
AC_2	STNA–230	GEN2–230	0.032	0.161	0.153	0	0.483
AC_3	GEN2–230	STNC–230	0.0085	0.072	0.0745	0	0.216
AC_4	STNC–230	GEN3–230	0.0119	0.1008	0.1045	0	0.302
AC_5	GEN3–230	STNB–230	0.039	0.17	0.179	0	0.51
AC_6	STNB–230	GEN1–230	0.017	0.092	0.079	0	0.276

4.2. Nine-node Power Network WSCC-Integrated Stability Program Simulation Three-Phase Ground Fault Characteristics Analysis

A three-phase ground fault occurs at 50% of the line between the GEN2–230 and STNC–230 nodes in the WSCC power system-integrated stabilization program nine-node network. The fault setting location is shown in Figure 13.
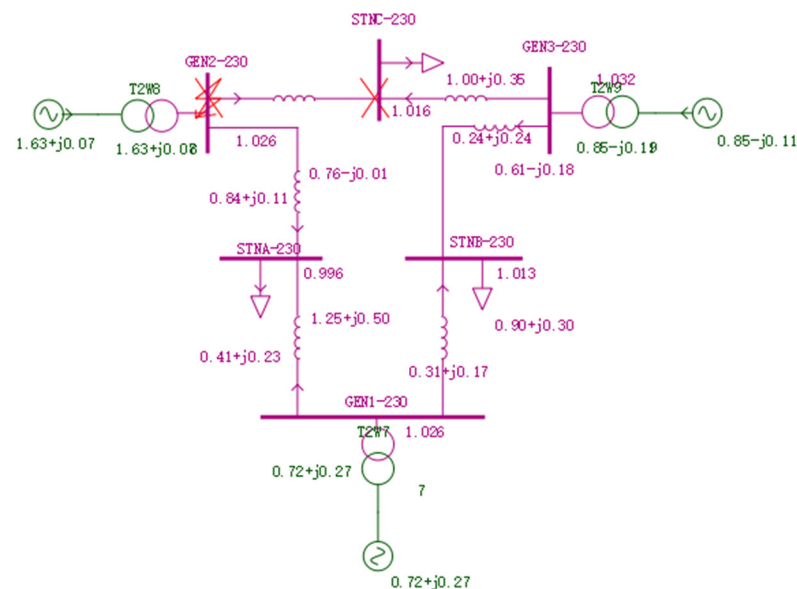
Figure 13. Power system-integrated stabilization program of WSCC nine-node fault location setting diagram.

After the occurrence of a 0.03 s fault, the voltage of nodes GEN1, GEN2, GEN3, GEN1–230, GEN2–230, GEN3–230, STNA–230, STNB–230, and STNC–230 all dropped to a large extent, and the voltage did not recover within 5 s after the fault occurred. At this moment, there is no risk prediction system based on digital twins involved in the system, and the specific degree of fall is shown in Figure 14. The relative power angles of the GEN1, GEN2, and GEN3 generators diverge, as shown in Figure 15. The system is unstable and risky after failure.
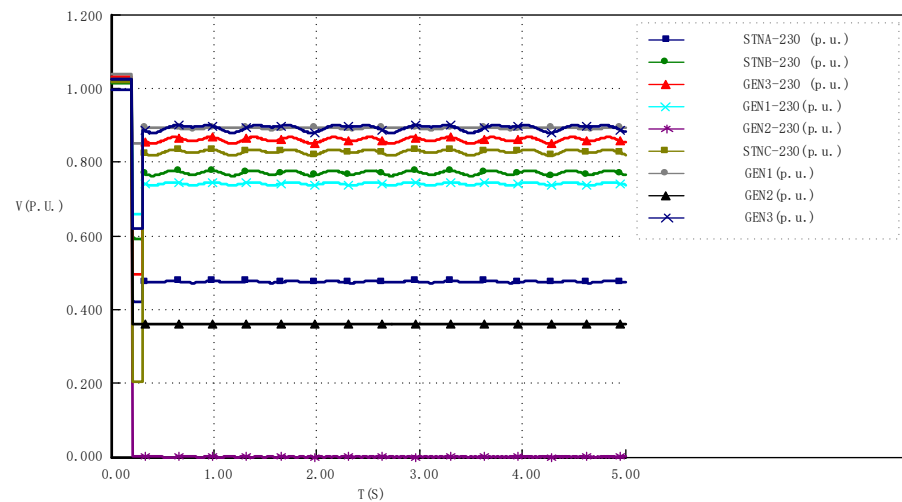
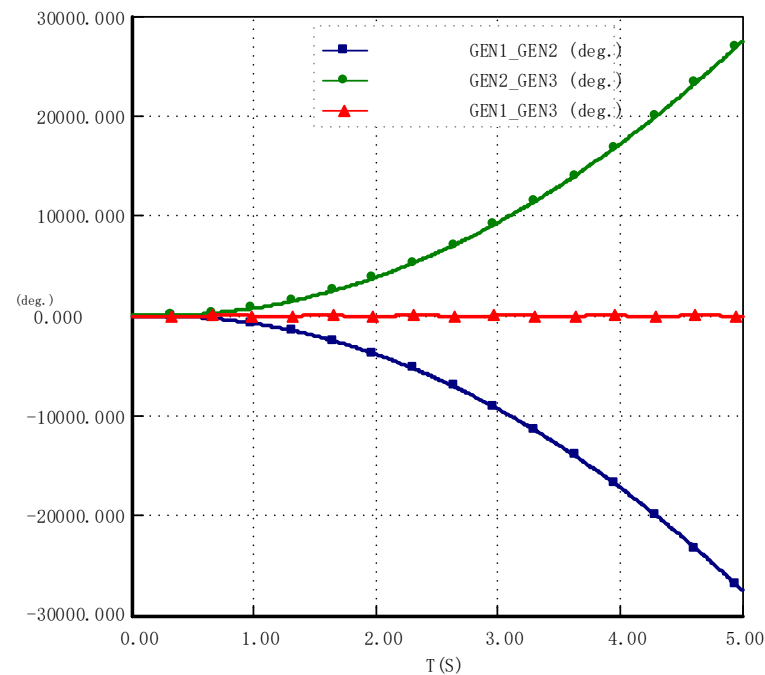**Figure 14.** Voltage data of each node in the nine-node WSCC network without the introduction of a power digital twin.

Figure 15. Relative power angles of GEN1, GEN2, and GEN3 network generators without the introduction of power digital twinning WSCC nine nodes.

4.3. Nine-Node Simulation Risk Prediction Based on Digital Twinning in WSCC Power System-Integrated Stability Program

Based on the digital twin in the integrated stability program of the WSCC nine-node power system simulated risk prediction, in order to obtain the operation parameters of the regional power system, the corresponding network model is established in PSASP, and the power flow calculation optimization analysis is carried out: sparse matrix, node coding optimization, tangent prediction vector unit processing. The active power and reactive power sensitivity are calculated for the regional power grid. According to the artificial neural network algorithm, the artificial modeling and calculation is carried out to determine the initial population and the calculation parameters of the neural network algorithm, namely the initial defense strategy of each node; the correction is made in PSASP. In the actual calculation process, the steady-state index in the objective function

is ignored, but only the transient index is retained. The objective function value is taken as the evaluation function value of each individual. The above calculation is performed for each individual in the initial population, the fitness of each individual is evaluated, the corresponding fitness of the optimal individual is recorded, and a new generation of the population is obtained by using the revolving gate of the neural network. The new population is taken as the initial population and the calculation is repeated. If the termination condition is met, that is, if the calculation times are sufficient or the solution is satisfactory enough, the optimal solution of the transient characteristics of each node is terminated

(1) Based on the power digital twin, the risk prediction and correction of the nine nodes of the integrated stability program WSCC, in the case of three-phase failure, are carried out. The specific fault location is 50% of the line between the two nodes GEN2–230 and STNC–230, as shown in Figure 13. After the occurrence of the 0.03 s fault, the nodes GEN1, GEN2, GEN3, GEN1–230, GEN2–230, GEN3–230, STNA–230, and STNB–230, STNC-230 can be obtained. After the voltage fluctuation occurs, the digital twinning algorithm quickly plays the role of balancing the voltage stability. As a result, the voltage of each node fluctuates within the stable threshold range. The specific degree of fluctuation is simulated in detail in Figure 16. The relative power angles of the GEN1, GEN2, and GEN3 generators do not diverge, as shown in Figure 17. Figures 16 and 17 prove that power flow calculation optimization and power digital twinning can effectively reduce the risk of regional power systems when a three-phase failure occurs between two nodes of nine nodes in the integrated WSCC power system stabilization program, based on power digital twinning.

(2) Based on the power digital twinning, the risk prediction and correction of the nine nodes of the WSCC integrated stability program in the case of phase-to-phase failure are carried out. The specific fault location is 50% of the line between the two nodes GEN2–230 and STNC–230, as shown in Figure 15. After the occurrence of the 0.03 s fault, the nodes GEN1, GEN2, GEN3, GEN1–230, GEN2–230, GEN3–230, STNA–230, STNB–230, and STNC–230 can be obtained. After the voltage fluctuation occurs, the digital twinning algorithm quickly plays the role of the balancing voltage stability. The voltage of each node fluctuates within the range of the stable threshold. The specific degree of fluctuation is simulated and analyzed in detail in Figure 18. The relative power angles of the GEN1, GEN2, and GEN3 generators do not diverge, as shown in Figure 19. Figures 18 and 19 prove that power flow calculation optimization and power digital twinning can effectively reduce the risk of regional power systems when nine nodes of the integrated WSCC power system stabilization program fail in phases between two nodes.
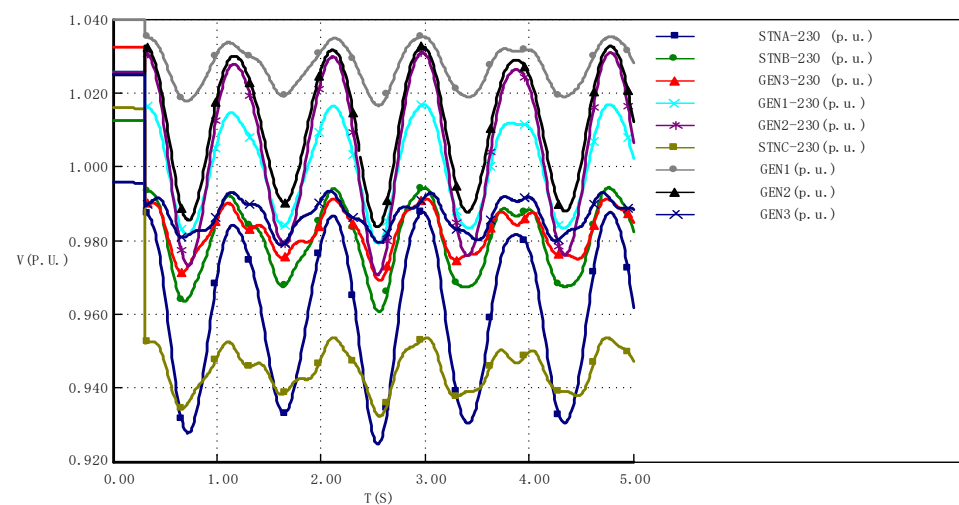

Figure 16. Voltage data of each node in the nine-node WSCC network under the introduction of a power digital twin three-phase fault.
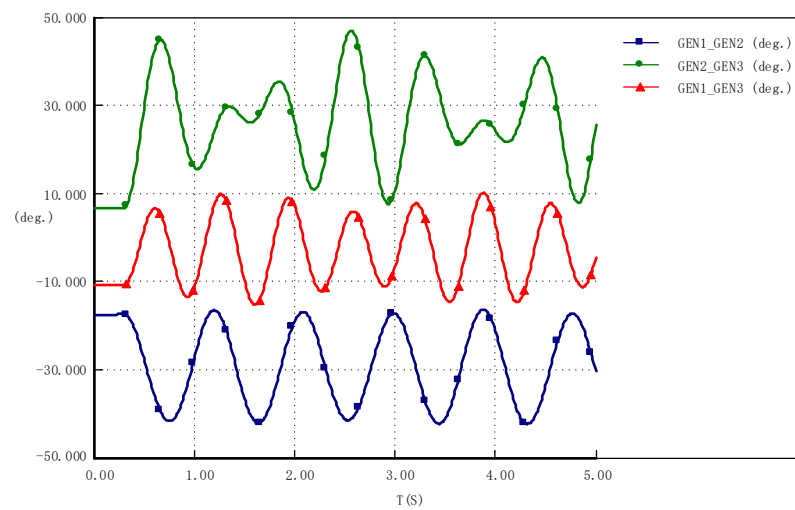
Figure 17. Relative power angle of GEN1, GEN2, and GEN3 motor under three-phase fault with the introduction of electric digital twinning.
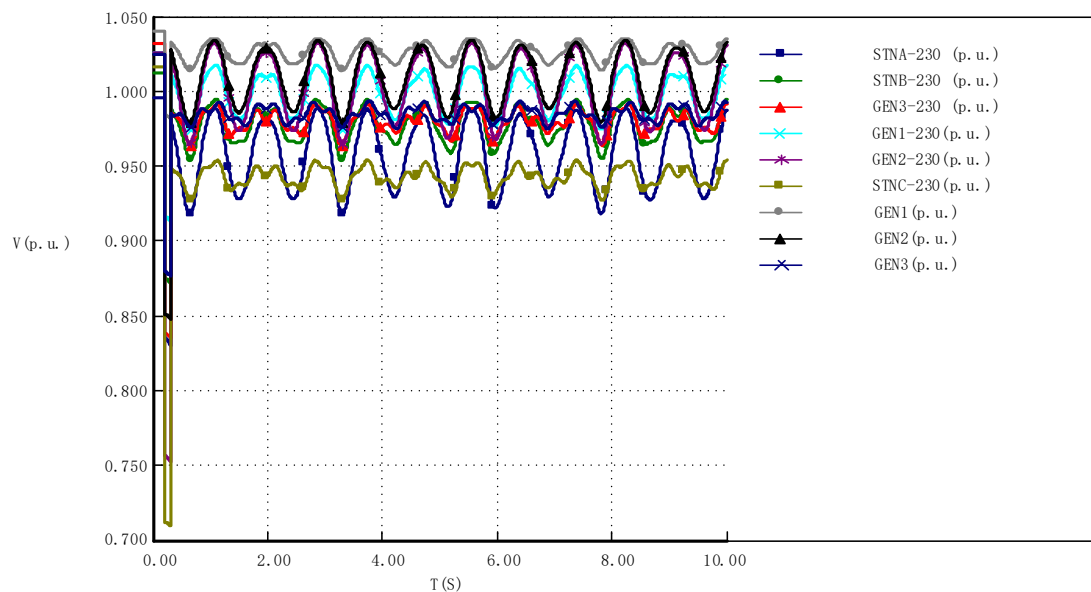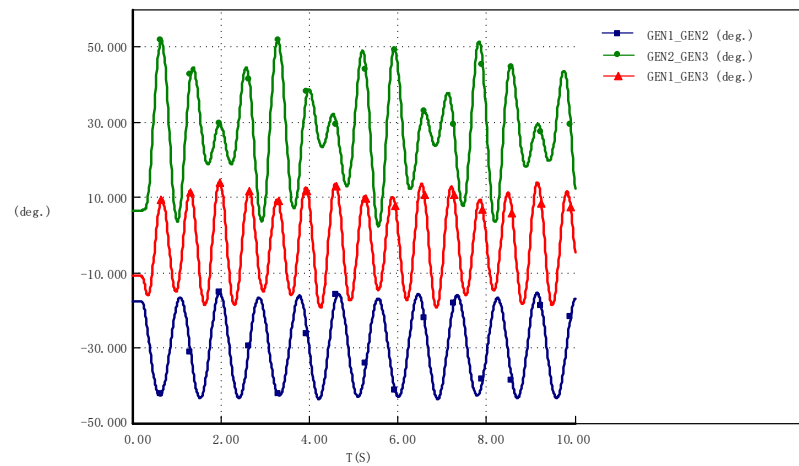

Figure 18. Voltage data of each node in the nine-node WSCC network under the introduction of a power digital twin phase fault.

(3) Based on the power digital twinning, the risk prediction and correction of the nine nodes of the integrated stability program of the WSCC power system, in the case of single-phase failure, are carried out. The specific fault location is 50% of the line between the two nodes GEN2–230 and STNC–230, as shown in Figure 15. After the occurrence of the 0.03 s fault, the nodes GEN1, GEN2, GEN3, GEN1–230, GEN2–230, GEN3–230, STNA–230, STNB–230, and STNC–230 can be obtained. After the voltage fluctuation occurs, the digital twinning algorithm quickly plays the role of balancing the voltage stability. The voltage of each node fluctuates within the range of the stable threshold. The specific degree of fluctuation is simulated and analyzed in detail in Figure 20. The relative power angles of the GEN1, GEN2, and GEN3 generators do not diverge, as shown in Figure 21. Figures 20 and 21 prove that power flow calculation optimization and power digital twinning can effectively reduce the risk of regional power systems when nine nodes of the integrated WSCC power system stabilization program fail in phases between two nodes.

Figure 19. Relative power angle of GEN1, GEN2, and GEN3 motor under the fault phase of an electric digital twin phase.
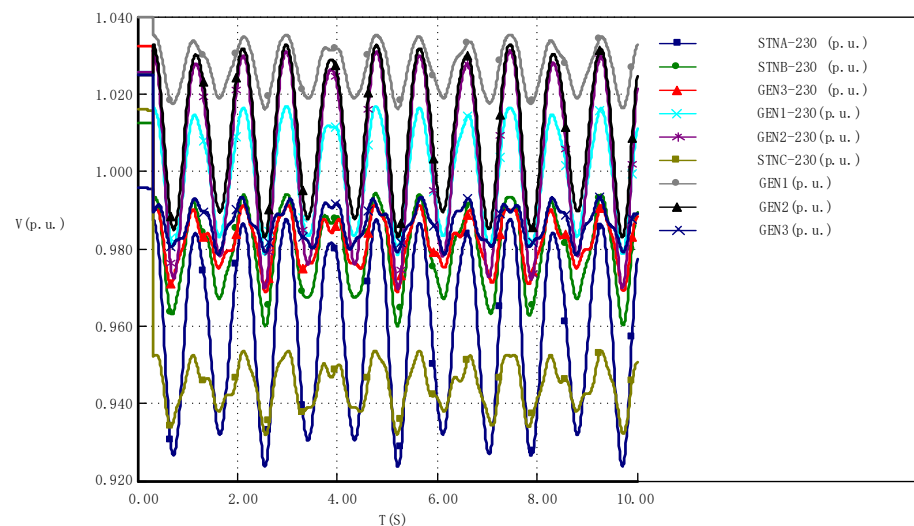

Figure 20. Voltage data of each node in the nine-node WSCC network with the introduction of a power digital twin single-phase fault.

Finally, the eigenvalue analysis of the nine-node model of the WSCC power system-integrated stabilization program after the adoption of power digital twinning is carried out. As shown in Figure 22, the coordinates of GEN1, GEN2, and GEN3 are all located on the X-axis, Therefore, it can be proven that the WSCC nine-node model is stable after adopting the research method described in this paper; this which further verifies that power flow calculation optimization and power digital twinning can effectively reduce the risk of the regional power system.

Future research will explore the application of power digital twin in more nodes, AC–DC hybrid systems, flexible DC systems, and add different operating conditions.
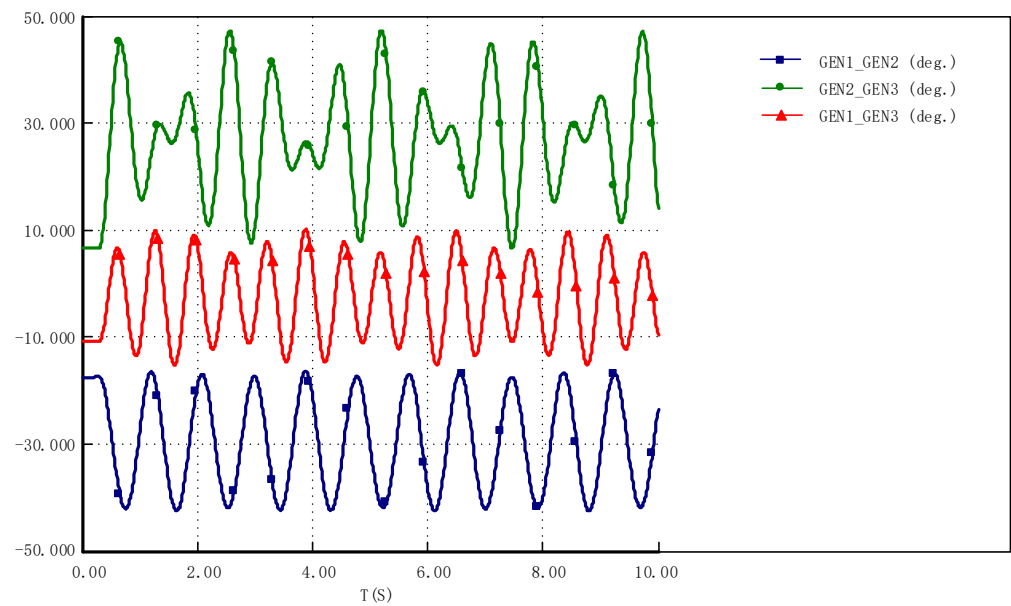
Figure 21. The relative power angle of GEN1, GEN2, and GEN3 with the introduction of an electric digital twinning single-phase fault motor.
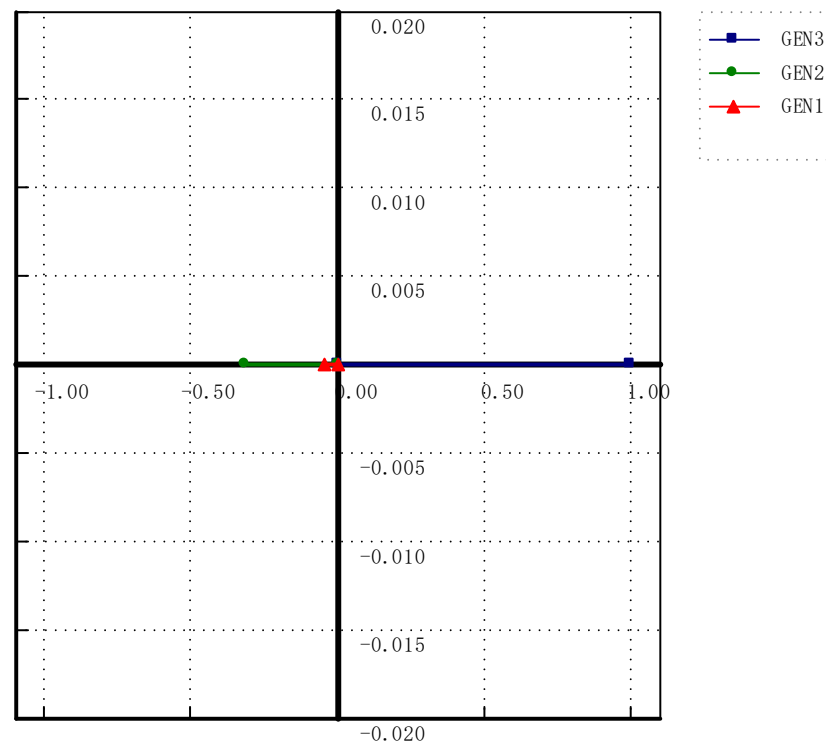

Figure 22. Analysis of characteristic values of GEN1, GEN2, and GEN3 motors under different faults after the introduction of electric digital twinning.

5. Conclusions

This paper predicts and analyzes the steady-state risks of complex power systems, based on the power digital twin. Firstly, power flow calculation and optimization are carried out for complex large power grid systems. Based on sparse matrix storage and node coding optimization, the power flow calculation speed is improved and the memory usage is reduced. The accuracy and timeliness of continuous power flow calculation when obtaining the node power and voltage are improved by using the unit processing

tangent prediction vector and the internal machine of the prediction vector to determine the prediction direction. According to the optimization results of the power flow calculation, the multi-objective optimization problem of the power system simulation is solved. Finally, power flow calculation optimization and neural network analysis are applied to the integrated stability program of the WSCC power system's nine-node model, in order to simulate the regional power grid for simulation analysis. Steady-state risk prediction and intervention are carried out for the three-phase faults, phase-to-phase faults, and single-phase faults of two nodes. The steady-state analysis is carried out on the voltage of nodes GEN1, GEN2, GEN3, GEN1–230, Gen2–230, GEN3–230, STNA–230, STNB–230, and STNC–230 under different working conditions, and on the relative power angle of generators GEN1, GEN2, GEN3 under different working conditions. It is found that the steady-state risk of the power system can be reduced and the stability of the power system can be improved, based on the power digital twin under different risks.

References

1. Zhou, X.; Chen, S.; Lu, Z.; Huang, Y.; Ma, S.; Zhao, Q. Technology features of the new generation power system in China. *Proc. CSEE* **2018**, *38*, 1893–1904. (In Chinese)
2. Yang, T.; Zhao, L.; Wang, C. Review on application of artificial intelligence in power system and integrated energy system. *Autom. Electr. Syst.* **2019**, *43*, 2–14. (In Chinese)
3. Tao, F.; Liu, W.; Zhang, M.; Hu, T.; Qi, Q.; Zhang, H.; Sui, F.; Wang, T.; Xu, H.; Huang, Z. Fivedimension digital twin model and its ten applications. *Engineering* **2019**, *25*, 1–18. (In Chinese)
4. Tao, F.; Zhang, H.; Liu, A.; Nee, A.Y. Digital twin in the industry: State-of-the-art. *IEEE Trans. Ind. Inform.* **2019**, *15*, 2405–2415. [CrossRef]
5. Tang, W.; Chen, X.; Qian, T.; Liu, G.; Li, M.; Li, L. Technologies and applications of a digital twin for developing smart energy systems. *Strateg. Study CAE* **2020**, *22*, 74–85. (In Chinese) [CrossRef]
6. Kritzinger, W.; Karner, M.; Traar, G.; Henjes, J.; Sihn, W. Digital twin in manufacturing: A categorical literature review and classification. *IFAC-PapersOnLine* **2018**, *51*, 1016–1022. [CrossRef]
7. Negri, E.; Berardi, S.; Fumagalli, L.; Macchi, M. MES-integrated digital twin frameworks. *J. Manuf. Syst.* **2020**, *56*, 58–71. [CrossRef]
8. Zhuang, C.; Gong, J.; Liu, J. Digital twin-based assembly data management and process traceability for complex products. *J. Manuf. Syst.* **2021**, *58*, 118–131. [CrossRef]
9. Rosen, R.; Von Wichert, G.; Lo, G.; Bettenhausen, K.D. About the importance of autonomy and digital twins for the future of manufacturing. *IFAC-PapersOnLine* **2015**, *48*, 567–572. [CrossRef]

10. Ladj, A.; Wang, Z.; Meski, O.; Belkadi, F.; Ritou, M.; Da Cunha, C. A knowledge-based Digital Shadow for the machining industry in a Digital Twin perspective. *J. Manuf. Syst.* **2021**, *58*, 168–179. [CrossRef]

11. Stark, R.; Kind, S.; Neumeyer, S. Innovations in digital modeling for next-generation manufacturing system design. *CIRP Ann.* **2017**, *66*, 169–172. [CrossRef]

12. González, M.; Salgado, O.; Croes, J.; Pluymers, B.; Desmet, W. A digital twin for operational evaluation of vertical transportation systems. *IEEE Access* **2020**, *8*, 114389–114400. [CrossRef]

13. Bie, Z.; Wang, X.; Hu, Y. Review and prospect of planning of energy Internet. *Proc. CSEE* **2017**, *37*, 6445–6462. (In Chinese)

14. Geidl, M.; Koeppel, G.; Favre-Perrod, P.; Klockl, B.; Andersson, G.; Frohlich, K. Energy hubs for the future. *IEEE Power Energy Mag.* **2007**, *5*, 24–30. [CrossRef]

15. Janko, S.; Johnson, N.G. Reputation-based competitive pricing negotiation and power trading for grid-connected microgrid networks. *Appl. Energy* **2020**, *277*, 115598. [CrossRef]

16. Wu, Y.; Zhang, K.; Zhang, Y. Digital twin networks: A survey. *IEEE Internet Things J.* **2021**, *8*, 13789–13804. [CrossRef]

17. Sierra-Arriaga, F.; Branco, R.; Lee, B. Security issues and challenges for virtualization technologies. *ACM Comput. Surv.* **2021**, *53*, 45. [CrossRef]

18. Tian, L.; Yang, M.Z.; Wang, S.G. An overview of computing first networking. *Int. J. Web Grid Serv.* **2021**, *17*, 81–97. [CrossRef]

19. Yuan, S. Research on time synchronization in wireless sensor networks. *Inf. Rec. Mater.* **2021**, *22*, 222–224.

20. Zhang, P.; Huang, B.; Ju, H. MBSE: Future direction of system engineering. *Sci. Technol. Rev.* **2020**, *38*, 21–26.

21. Gyongyosi, L. Objective function estimation for solving optimization problems in gate-model quantum computers. *Sci. Rep.* **2020**, *10*, 14220. [CrossRef] [PubMed]

22. Zhang, P.; Li, T.; Wang, G.; Luo, C.; Chen, H.; Zhang, J.; Wang, D.; Yu, Z. Multi-source information fusion based on rough set theory: A review. *Inf. Fusion* **2021**, *68*, 85–117. [CrossRef]

23. Liu, Y.; Wang, Q.; Xu, Z. Research on data cleaning and abnormal recognition method of dissolved gas in oil based on multi-layer architecture. *J. North China Electr. Power Univ. (Nat. Sci. Ed.)* **2022**, *49*, 81–89.

24. Pu, T.; Chen, S.; Zhao, Q. Framework design and application prospect for digital twins system of energy internet. *Proc. CSEE* **2021**, *41*, 2012–2028.

25. Chen, Y.B. Integrated and intelligent manufacturing: Perspectives and enablers. *Engineering* **2017**, *3*, 588–595. [CrossRef]

26. El Marai, O.; Taleb, T.; Song, J. Roads infrastructure digital twin: A step toward smarter cities realization. *IEEE Netw.* **2021**, *35*, 136–143. [CrossRef]

27. Wang, N.; Zhao, F. An assessment of the condition of distribution network equipment based on large data fuzzy decision-making. *Energies* **2020**, *3*, 197. [CrossRef]

28. Giannaros, E.; Kotzakolios, A.; Kostopoulos, V.; Sotiriadis, G.; Vignjevic, R.; Djordjevic, N.; Boccaccio, M.; Meo, M. Low- and high-fidelity modeling of sandwich-structured composite response to a bird strike, as tools for a digital-twin-assisted damage diagnosis. *Int. J. Impact Eng.* **2022**, *160*, 104058. [CrossRef]

29. Ren, Z. Digital high-efficiency energy-saving solution, helping to achieve the "Double carbon" goal-interview Qi Luping, head of ABB's Motion Control Division in China. *Electr. Age* **2022**, *13*, 6–8.

30. Ma, X.; Shen, W.; Zhen, W. A study on the optimal scheduling strategy of an electric-gas-thermal integrated energy system based on low carbon target. *Power Syst. Clean Energy* **2021**, *37*, 116–122. (In Chinese)

31. Zhang, N.; Ma, G.; Guan, Y. Panoramic information perception and intelligent grid. *Proc. CSEE* **2021**, *41*, 1274–1283. (In Chinese)

32. Zhou, M.; Yan, J.; Wu, Q. Graph computing and its application to power grid analysis. *CSEE J. Power Energy Syst.* **2022**. [CrossRef]

33. Yan, Y.; Tao, H.; Li, Y. Research and practice of integration of information in power dispatching center. *Relay* **2007**, *1*, 37–40. (In Chinese)

34. Zhou, E.; Feng, D.; Wu, Z. In-memory computing and its application to power system analysis. *Autom. Electr. Power Syst.* **2017**, *41*, 1–7. (In Chinese)

35. Zhou, E.; Feng, D.; Yan, J. A software platform for second-order responsiveness power grid online analysis. *Power Syst. Technol.* **2020**, *44*, 3474–3480. (In Chinese)

36. Qi, B.; Zhang, P.; Zhang, S. Application status and development prospects of digital twin technology in the condition assessment of power transmission and transformation equipment. *High Volt. Eng.* **2021**, *47*, 1522–1538. (In Chinese)

37. Danilczyk, W.; Sun, Y.; He, H. ANGEL: An intelligent digital twin framework for microgrid security. In Proceedings of the 2019 North American Power Symposium (NAPS), Wichita, KS, USA, 13–15 October 2019.

38. Shen, C.; Jia, M.; Chen, Y.; Huang, S.; Xiang, Y. Digital twin of the energy internet and its application. *J. Glob. Energy Interconnect.* **2020**, *3*, 1–13. (In Chinese)

39. Makihata, M.; Matsushita, K.; Pisano, A.P. MEMS-based non-contact voltage sensor with multi-mode resonance shutter. *Sens. Actuators A Phys.* **2019**, *294*, 25–36. [CrossRef]

40. Erol-Kantarci, M.; Mouftah, H.T. Wireless multimedia sensor and actor networks for the next generation power grid. *Ad Hoc Netw.* **2011**, *9*, 542–551. [CrossRef]

41. Zeng, M.; Wang, Y.; Li, M.; Dong, H.; Zhang, X. Preliminary study on the architecture and implementation plan of widespread power internet of things. *Smart Power* **2019**, *47*, 1–7.

42. Morello, R.; De Capua, C.; Fulco, G.; Mukhopadhyay, S.C. A smart power meter to monitor energy flow in smart grids: The role of advanced sensing and IoT in the electric grid of the future. *IEEE Sens. J.* **2017**, *17*, 7828–7837. [CrossRef]

43. Abe, R.; Taoka, H.; McQuilkin, D. Digital grid: Communicative electrical grids of the future. *IEEE Trans. Smart Grid* **2011**, *2*, 399–410. [CrossRef]

44. Abe, R. Digital grid: Full of renewable energy in the future. In Proceedings of the 2016 IEEE International Conference on Consumer Electronics-Taiwan, Taiwan, China, 27–29 May 2016; pp. 104–106.

45. Shi, P. The concept, development form, and significance of digital twin. *Softw. Integr. Circuit* **2018**, *1*, 30–33.

46. Wang, J.; Cui, H.; Hao, H.; Yao, H.; Bao, L. Research on digital power grid information integration solution. *MATEC Web Conf.* **2018**, *173*, 03026. [CrossRef]

47. Zhuang, C.; Liu, J.; Xiong, H.; Ding, X.; Liu, S.; Weng, G. Connotation, architecture, and trends of product digital twin. *Comput. Integr. Manuf. Syst.* **2017**, *23*, 753–768.

48. Liu, D.; Guo, K.; Wang, B.; Peng, Y. Summary and perspective survey on digital twin technology. *Chin. J. Sci. Instrum.* **2018**, *39*, 1–10.

49. Liu, Y.; Xu, Z.; Li, G.; Xia, Y.; Gao, S. Review on applications of artificial intelligence-driven data analysis technology in condition-based maintenance of power transformers. *High Volt. Eng.* **2019**, *45*, 337–348.

50. Tang, W.; Niu, Z.; Zhao, B. Research and application of data-driven artificial intelligence technology for condition analysis of power equipment. *High Volt. Eng.* **2020**, *46*, 2985–2999.

51. Li, P.; Bi, J.G.; Yu, H.; Xu, Y. Technology and application of intelligent sensing and state sensing for transformation equipment. *High Volt. Eng.* **2020**, *46*, 3097–3113.

52. Maja, H.T.; Rajib, D.; Ljubisa, S.; Xu, S.; Philip, C.; Gary, M.; Brian, R.; Paul, S.; Jian, D.; Tony, F. Design and testing of a modular sic-based power block. In Proceedings of the International Exhibition and Conference for Power Electronics, Intelligent Motion, Renewable Energy and Energy Management, Nuremberg, Germany, 9–11 September 2021; pp. 1–4.

53. Negri, E.; Fumagalli, L.; Macchi, M. A review of the roles of the digital twin in CPS-based production systems. *Procedia Manuf.* **2017**, *11*, 939–948. [CrossRef]

54. Zhou, S.; Xie, L.; Song, R. Building and application of substation digital construction management platform based on BIM. *Electr. Power* **2019**, *52*, 142–147.

55. Tian, F.; Duan, H.; Yang, Z. *White paper on digital twin technology*; Laboratory of Digital Twins, Pera Global Technology Co., Ltd.: Beijing, China, 2019.

56. Glaessgen, E.; Stargel, D. The digital twin paradigm for future NASA and U.S. air force vehicles. In Proceedings of the AIAA/ASME/ASCE/AHS/ASC Structures, Structural Dynamics and Materials Conference—Special Session on the Digital Twin, Honolulu, HI, USA, 19 April 2012.

57. Zengin, U.; Durak, U.; Hartmann, S. The digital twin paradigm for aircraft-review and outlook. In Proceedings of the AIAA SciTech Forum, Online, 6 January 2020.

58. Edward, K. The US air force digital thread/digital twin-life cycle integration and use of computational and experimental knowledge. In Proceedings of the 54th AIAA Aerospace Sciences Meeting, San Diego, CA, USA, 4–8 January 2016.

59. Shi, L.; Jian, Z. Vulnerability assessment of cyber-physical power system based on dynamic attack-defense game model. *Autom. Electr. Power Syst.* **2016**, *40*, 99–105.

60. Bie, Z.; Lin, Y.; Qiu, A. Concept and research prospects of power system resilience. *Autom. Electr. Power Syst.* **2015**, *39*, 1–9.

61. Pan, S.; Morris, T.; Adhikari, U. Developing a hybrid intrusion detection system using data mining for power systems. *IEEE Trans. Smart Grid* **2015**, *6*, 3104–3113. [CrossRef]

62. Luo, Z.; Yang, X.; Sun, G. Finite automation intrusion tolerance system model based on Markov. *J. Commun.* **2019**, *40*, 79–89.

63. Deng, R.; Zhuang, P.; Liang, H. CCPA: Coordinated cyber-physical attacks and countermeasures in smart grid. *IEEE Trans. Smart Grid* **2017**, *8*, 2420–2430. [CrossRef]

64. Xue, Y.; Li, M.; Luo, J.; Ni, M.; Chen, Q. Modeling method for coupling relations in cyber-physical power systems based on correlation characteristic matrix. *Autom. Electr. Power Syst.* **2018**, *42*, 11–19.